DOI 10.1007/s11085-017-9717-5

Relevance of Other Parameters than Carbon Activity in Defining the Severity of a Metal Dusting Environment

Aurélie Rouaix-Vande Put[1] · Aurélien Fabas[1] · Sébastien Doublet[2] · Daniel Monceau[1]

Abstract Two metal dusting experiments were carried out at 570 °C on 800HT and HR120 alloys, for more than 6000 h. The tests were designed to run at different total pressures and gas velocities but similar carbon activities and oxygen partial pressures. For a given alloy, shorter average incubation times and larger mass losses were observed at high pressure. For both tests, HR120 alloy underwent greater mass losses and exhibited a higher pit density. For nearly all samples, pit densities greatly differed between both sides of the specimens. Therefore, the carbon and oxygen activities alone are not sufficient to evaluate the aggressiveness of a metal dusting environment. Greater degradation was the result of the association of a higher gas velocity with a higher total pressure and a finer alloy grain size.

Keywords Metal dusting · Pitting · Modelling · Water vapor · Pressure

✉ Aurélie Rouaix-Vande Put
aurelie.rouaix@ensiacet.fr

Aurélien Fabas
aurelien.fabas@ensiacet.fr

Sébastien Doublet
sebastien.doublet@airliquide.com

Daniel Monceau
daniel.monceau@ensiacet.fr

[1] CIRIMAT, Université de Toulouse, CNRS, INPT, UPS, ENSIACET, 4 allée Emile Monso, BP-44362, 31030 Toulouse Cedex 4, France

[2] Air Liquide R&D, Centre de Recherche Paris-Saclay, 1 chemin de la porte des loges, BP-126, 78354 Jouy-en-Josas Cedex, France

Introduction

The accurate lifetime prediction of plant materials operating at high pressures in severe and complex atmospheres constitutes a significant challenge. An overestimation would result in unplanned plant shutdowns causing major risks in terms of safety and process reliability. Underestimation is also not desirable due to the early replacement of fit-for-service parts which leads to unplanned expenses. Coping with temperatures between 400 and 800 °C in highly carburizing environments and under high pressures, some parts of syngas production units are exposed to the "metal dusting" degradation mechanism. Metal dusting is a catastrophic corrosion phenomenon that leads to the disintegration of metallic materials, characterized by the formation of a carbon-rich deposit called "coke" which contains metallic particles, oxides and carbides [1]. For protective oxide forming metallic alloys, this degradation mechanism is characterized by localized pitting at the defects of the oxide scale after a given incubation period.

Running high pressure tests under severe environments is a real challenge. In the literature, the majority of experimental results were obtained at atmospheric pressure, for short exposure times and under environments containing low water vapor levels, which makes the transposition to industrial conditions difficult. To this end, carbon activity is generally used to define metal dusting conditions. However, a given carbon activity can be obtained from very different conditions of pressure, temperature and gas mixture [2, 3]. To better understand what governs the severity of metal dusting, two experiments were carried out on two austenitic commercial alloys, 800HT and HR120, for more than 6000 h. They were performed at the same temperature, similar carbon activities and oxygen partial pressures but with different total pressures and gas velocities.

Experimental Procedures

Two metal dusting experiments were carried out at 570 °C. One was performed at 21 bar with a $CO–H_2–H_2O–CH_4–CO_2$ gas mixture and a gas flow of 2.8 mm/s while the other one was carried out at 1 bar using a $CO–H_2–H_2O$ environment and a much lower gas velocity, Table 1. The gas composition of the 1 bar experiment was adjusted to obtain similar carbon and oxygen activities for both tests. Carbon and oxygen activities were determined using the syngas reaction and the water decomposition reaction respectively, and considering a perfect gas behavior, see Table 2 for details on the formula.

Two austenitic commercial alloys, 800HT and HR120, were tested in both conditions. For a given alloy, the sample batch differs between experiments. The

Table 1 Conditions of metal dusting tests

Test at 570 °C	Gas composition (%vol)					Gas velocity (mm/s)	Gas flow (ml/min/cm^2)	a_c	P_{O_2} bar
	CO	H_2	H_2O	CH_4	CO_2				
1 bar	47.25	47.25	5.5	–	–	0.018	13.4	32.0	2.09×10^{-27}
21 bar	12.80	49.10	33.4	1.6	3.1	2.8	530	31.2	7.15×10^{-26}

composition of each alloy and batch is given in Table 3 in atomic percent. It was determined by optical emission spectroscopy for samples tested at 1 bar and by energy dispersive spectroscopy based on real standard for alloys exposed to the high pressure experiment. Their grain size, measured by image analysis on etched samples, is reported in Fig. 1. Prior to testing, the sample surfaces were ground using P600 SiC grit paper, the edges were chamfered and the samples were ultrasonically cleaned in acetone and ethanol successively. Discs of 14 mm diameter (with a hole drilled in the middle) were positioned on alumina sticks in the vertical rig operating at high

Table 2 Formula for the determination of a_c and P_{O_2}

Reaction	ΔG° (J/mol)	Formula considering perfect gases	Formula considering real gases
Syngas reaction			
$CO + H_2 = C + H_2O$	$-134515 + 142.37T$	$a_c = \frac{P_{CO}P_{H_2}}{P_{H_2O}P^\circ} e^{\left(-\frac{\Delta G^\circ}{RT}\right)}$	$a_c = \frac{\varphi_{CO}\varphi_{H_2}}{\varphi_{H_2O}} \frac{P_{CO}P_{H_2}}{P_{H_2O}P^\circ} e^{\left(-\frac{\Delta G^\circ}{RT}\right)}$
Water decomposition			
$H_2O = H_2 + {}^1/_2O_2$	$246440 - 54.8T$	$P_{O_2} = \left(\frac{P_{H_2O}}{P_{H_2}} e^{\left(-\frac{\Delta G^\circ}{RT}\right)}\right)^2$	$P_{O_2} = \frac{1}{\varphi_{O_2}} \left(\frac{\varphi_{H_2O}}{\varphi_{H_2}} \frac{P_{H_2O}}{P_{H_2}} e^{\left(-\frac{\Delta G^\circ}{RT}\right)}\right)^2$

ΔG° is the standard free energy change, function only of temperature T expressed in K. P° is the standard pressure equal to 1 bar

φ_i is the fugacity coefficient of the gas i

Table 3 Alloy composition in at %

Alloy	Test	Ni	Fe	Cr	Al	Co	Mo	Nb	Mn	Si	Ti	Cu	Others
800HT	1 bar	31.5	43.6	20.8	0.9	0.1	0.2	–	1.0	0.7	0.5	0.2	0.24C, 0.03P, 0.24 N
	21 bar	28.4	45.3	22.4	1.3	–	–	–	0.8	1.0	0.6	0.2	C, S, P
HR120	1 bar	38.3	33.3	25.6	0.2	–	0.1	0.4	0.8	0.8	–	0.1	0.33C, 0.06P, 0.02 N
	21 bar	34.4	34.8	27.8	0.1	–	0.1	0.5	0.9	1.3	0.1	–	C, B, N

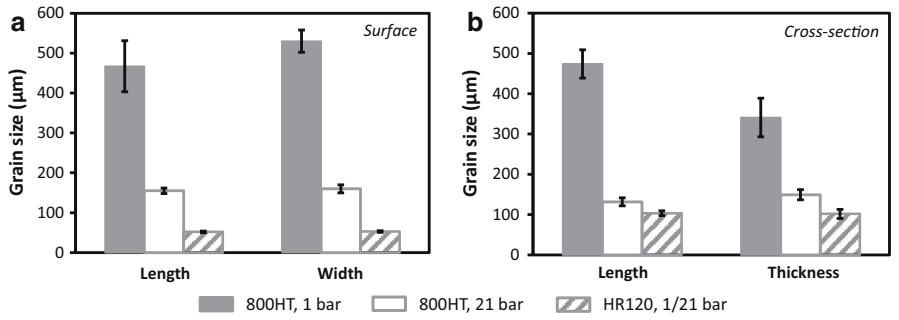

Fig. 1 Alloy grain size measured by image analysis on **a** the surface and **b** the cross-section. For measurements at the surface of the circular samples tested at 21 bar, length and width are two normal directions

pressure. Rectangular specimens (10 × 20 mm) were laid on an alumina sample holder in the horizontal rig operating at atmospheric pressure. The mass change control was done by weighting the samples three times every 500 h approximately. More information on the experimental procedure and rigs can be found in [4] for the atmospheric pressure (AP) test and in [5] for the high pressure (HP) test.

Secondary electron microscopy (SEM) observations of the surface and cross-section of corroded samples were performed with a LEO 435VP microscope using the secondary electron imaging mode (SE) or the backscattered imaging mode (BSE). Some samples were also observed with a SEM/FIB FEI HELIOS 600i microscope using a 5 keV accelerating voltage.

Results and Discussion

The mass changes measured during both experiments are shown in Fig. 2. Whichever the alloy and the metal dusting test, the samples underwent a large mass loss after an incubation period. For both alloys, the mass losses were greater during the HP test than during the AP experiment. For both tests, HR120 alloy underwent

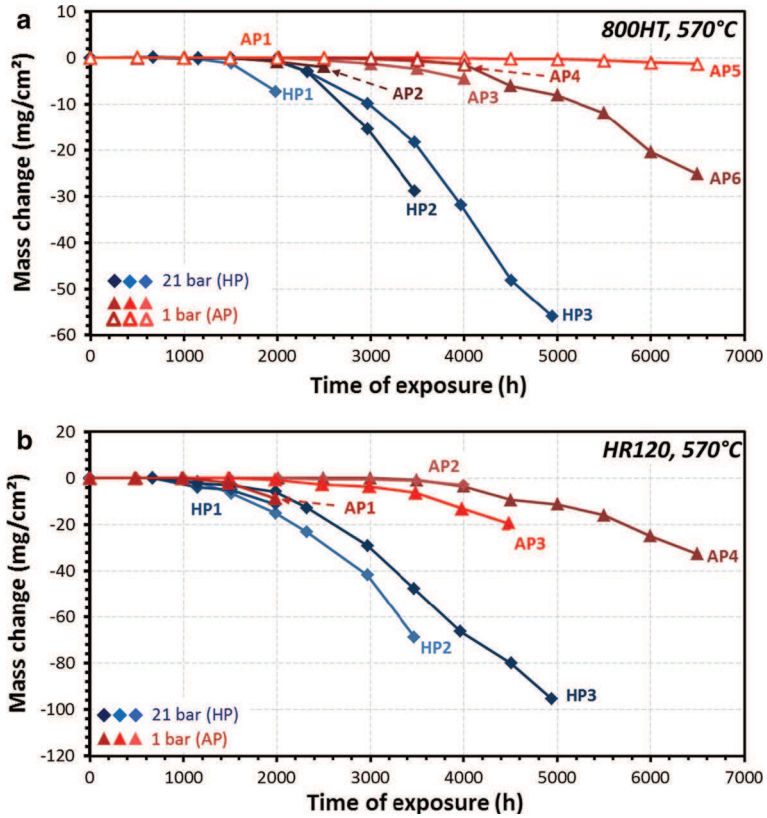

Fig. 2 Mass changes versus exposure time during metal dusting tests for **a** 800HT and **b** HR120 alloys

larger mass losses than 800HT. As previously mentioned, pictures of samples were taken after every removal, that being every 500 h of test approximately. Image analysis was performed on both sides of each sample. To avoid possible edge effects, the sample areas located 1 mm or less from the sample edges were excluded from this analysis. The pit density was monitored over time, Fig. 3, as well as the pit diameter evolution. Pit diameter measurements enabled to determine the lateral pit growth rate constant and the incubation time for each pit by extrapolating backwards to a zero size the pit growth kinetics. The obtained mean values are reported for both alloys in Fig. 4. More results related to the 800HT alloy exposed to the HP experiment and more details on the image analysis carried out to obtain the lateral pit growth rate constants and pit densities are described in [5].

First, the average incubation times do not allow to differentiate the alloy behavior for a given test, Fig. 4a, b. However, it clearly appears that the average incubation times were shorter for the HP test than for the AP experiment, regardless the side of the sample. Secondly, the evolution of the pit density mainly followed a continuous law under AP, while it did not depend on time under HP, Fig. 3. Besides, the pit density was generally higher on the internal side of the sample for the AP test (i.e. side facing the sample-holder) and on the external side of the sample for the HP test (i.e. side facing the furnace). Furthermore whichever the test, the pit density was larger for HR120 alloy than for 800HT. Finally, a large dispersion among samples is observed in the average lateral pit growth rate constants, making it difficult to compare alloys or sample sides. However, the average lateral pit growth rate

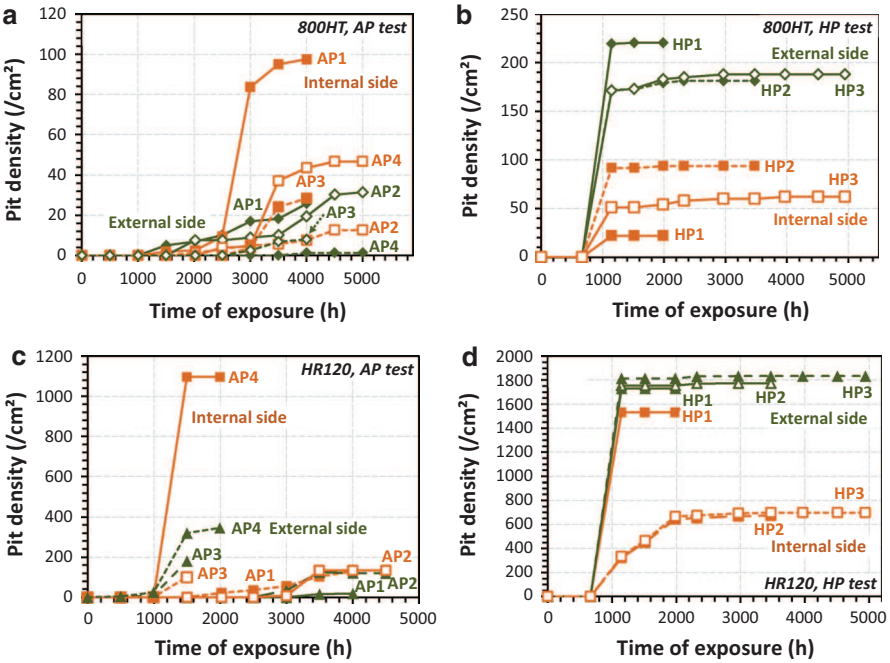

Fig. 3 Pit density versus exposure time for 800HT at **a** 1 bar and **b** 21 bars and for HR120 at **c** 1 bar and **d** 21 bar

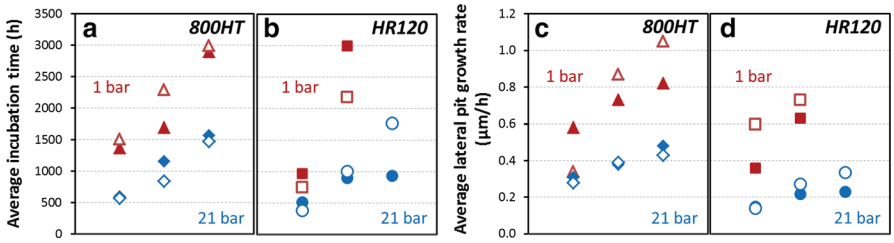

Fig. 4 For both tests, average incubation times for **a** 800HT and **b** HR120 samples and average lateral pit growth rate constants for a given side of **c** 800HT and **d** HR120 samples. *Full* and *empty symbols* are data obtained on the external and internal side of the samples respectively

constants were lower for the HP experiment than for the AP test. Such a difference can be explained by pit morphologies which greatly differed between both experiments, Fig. 5. A summary of grain sizes, average incubation times and average lateral pit growth rate constants for each alloy and test is available in Table 4.

While a succession of circular corrosion rings were observed on the surface of attacked samples exposed to the AP test, Fig. 5a, circular pits with a homogeneous composition of corrosion products were visible on the surface of samples exposed to HP, Fig. 5b. Besides, pits formed at AP exhibited a planar pit/alloy interface whereas the pits developed at HP presented a spherical cap shape, with a depth/diameter ratio equal to 1/5 and 1/6 for alloys 800HT and HR120 respectively (more details on pit characterization and formation mechanism of such concentric rings can be found in [4]).

Using the arc length formula in a circle, the corroded length, L_{corr}, can then be estimated for pits formed at 21 bar, based on the measured diameters and according to Eqs. 1 to 3.

$$L_{corr} = r\theta \tag{1}$$

with

$$r = \frac{p}{2} + \frac{d^2}{8p} \tag{2}$$

and

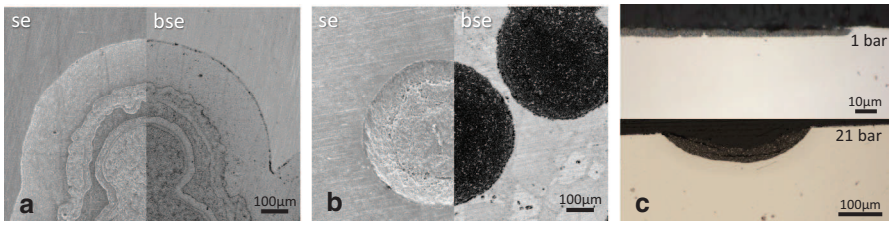

Fig. 5 Surface of a pit formed on 800HT alloy **a** at 1 bar after 4000 h and **b** at 21 bar after 1987 h. **c** Cross-sections of pits formed at 1 and 21 bar. **a**, **b** are SEM images while **c** displays optical images

Table 4 Grain sizes, average incubation times and average lateral pit growth rate constants for both alloys and both tests

	800HT				HR120			
	AP test		HP test		AP test		HP test	
	1 bar, 0.018 mm/s		21 bar, 2.8 mm/s		1 bar, 0.018 mm/s		21 bar, 2.8 mm/s	
	Surface	Cross-section	Surface	Cross-section	Surface	Cross-section	Surface	Cross-section
Grain size—length (μm)	467 ± 64	474 ± 35	155 ± 7	132 ± 10	52 ± 2	103 ± 6	73 ± 7	100 ± 6
Grain size—width/thickness (μm)	530 ± 28	341 ± 48	160 ± 10	149 ± 13	53 ± 2	102 ± 11	66 ± 4	106 ± 11
	Internal side	External side	Internal side	External side	Internal side	External side	Internal side	External side
Average incubation time (h)	1511	1370	565	596	755	970	381	514
	2287	1696	843	1154	2187	2997	1012	901
	2993	2900	1475	1566			1772	938
Average lateral pit growth rate constant (μm/h)	0.34	0.58	0.28	0.31	0.60	0.36	0.14	0.15
	0.87	0.73	0.39	0.38	0.73	0.63	0.27	0.22
	1.05	0.82	0.43	0.48			0.34	0.23

$$\theta = 2\arcsin\left(\frac{d}{2r}\right) \tag{3}$$

where r is the radius of the circle and θ the central angle of the arc. Factors equal to 1.10 and 1.07 were calculated between the corroded length and the measured diameter (considering p/d ratios of 1/5 and 1/6 for 800HT and HR120 respectively). Such values cannot justify the gap observed in the lateral pit growth rate constants. Thereafter, pit volumes were evaluated. As the pit depth is much smaller than the pit diameter measured at AP, the following formula can be used to estimate the pit volume:

$$V = \pi\left(\frac{d}{2}\right)^2 \times p \tag{4}$$

where d is the pit diameter and p the pit depth.

Based on spherical cap morphology, the volume of pits developed during the HP test was evaluated with the formula:

$$V = \frac{\pi \times p}{6} \quad 3\left(\frac{d}{2}\right)^2 + d^2\Bigg) \tag{5}$$

Considering a diameter of 1 mm, a maximum pit depth of 70 μm (see [4]) for pits formed at 1 bar, and a p/d ratio equal to 1/5 and 1/6 for alloys 800HT and HR120 respectively for pits formed at 21 bar, a ratio of 33 and 28 is obtained comparing the volumes of spherical cap shaped pits and plateau shaped pits. Such values are greater than the ratio observed between the average lateral pit growth rate constants of both tests. Hence, the larger mass losses measured for the HP test compared to the AP test resulted from greater pit densities and pit volumes.

However, the metal dusting tests were designed to obtain similar carbon activities and oxygen partial pressures, therefore, this cannot justify the differences observed between the experiments. Carbon activity and oxygen partial pressure were calculated considering a gas mixture composed of perfect gases. This hypothesis can be easily validated for the AP test but one can wonder if such an assumption is still acceptable at 21 bar. While the standard free energy change is function only of the temperature, fugacity coefficients (φ) were determined for each gas at 570 °C, 21 bar and for the injected gas mixture, with the Peng Robinson equation of state [6] using Simulis Thermodynamics® software. O_2 was not taken into account in the gas mixture as its content is so low that its fugacity coefficient φ_{O_2} can easily be considered equal to 1. The obtained values are reported in Table 5 and were used to evaluate the carbon activity and the oxygen partial pressure considering a real gas behavior, see the formula in Table 2. As the fugacity coefficients are close to 1, the resulting factors to apply to carbon activity and oxygen partial pressure, $\varphi_{CO}\varphi_{H_2}/\varphi_{H_2O}$ and $(\varphi_{H_2O}/\varphi_{H_2})^2/\varphi_{O_2}$, are 1.023 and 0.972 respectively. Thus, such thermodynamic calculations cannot explain the differences observed between both tests. It is interesting to mention that this factor was equal to 1.032 and 1.065 for a total pressure of 30 and 60 bar respectively. When considering a perfect gas

Table 5 Fugacity coefficients calculated at 570 °C, 21 bar and for a 12.8CO-49.1H_2-33.4H_2O-1.6CH_4-3.1CO_2 gas composition, with the Peng Robinson equation of state [6] using Simulis Thermodynamics® software

Test at 570 °C	Fugacity coefficients					a_c	P_{O_2} bar
	CO	H_2	H_2O	CH_4	CO_2		
21 bar	1.0085	1.0054	0.9914	1.0048	1.0037	31.9	7.05×10^{-26}

behavior, the higher the total pressure is, the greater the error on the carbon activity assessment is. However, these errors are below 10% for pressures used in industrial processes.

Since these samples were cut from different batches, the alloy composition and microstructure could play a role in the degradation, resulting from the oxidation of internal carbides, as detailed in [4]. However, the low batch composition variations cannot explain such a difference. Besides, the difference in composition between 800HT and HR120 cannot justify the greater degradation observed for HR120 alloy. With a lower concentration in Fe [7, 8] and a higher Cr content [9], HR120 should be more resistant to metal dusting. As carburization and oxidation of internal carbides are diffusion controlled phenomena, another explanation could come from different carbon and oxygen diffusion coefficients. While 800HT samples exposed to the HP experiment had a finer grain size than those tested at AP, HR120 samples exhibited similar grain size for both tests, and smaller than those of 800HT batches. It is generally admitted that a finer microstructure favors the formation of a protective oxide scale, thus preventing metal dusting attack [10]. This is thought to be due to an enhanced Cr diffusion through diffusion short circuits. However, at 570 °C, carbon and oxygen diffusion coefficients are several orders of magnitude greater than the diffusion coefficient of Cr in 800 alloys. The O diffusion coefficient is estimated to be 3.37×10^{-12} and 2.23×10^{-10} cm^2/s in Ni and γ-Fe based on data from [11, 12] respectively. C diffusion coefficient is comprised between 4.1×10^{-10} and 3.8×10^{-10} cm^2/s according to data on Fe-19Ni, Fe-49Ni and Fe-69Ni alloys exposed to higher temperatures [13]. For the 800 alloy, it is estimated to be between 2.3×10^{-13} and 2.5×10^{-11} cm^2/s [14]. Cr diffusion coefficients of 65Fe-14Cr-20Ni, 40Fe-15Cr-45Ni and 33Fe-22Cr-45Ni alloys, calculated at 570 °C, are comprised between 5.9×10^{-19} and 2.2×10^{-18} cm^2/s [15]. The Cr diffusion coefficient in the 800 alloy, estimated using data from Paul et al. [14], is equal to 5.0×10^{-22}, and 2.2×10^{-16} cm^2/s in grain boundaries. It is then proposed that, once the oxide scale is damaged, a finer microstructure favors carbon and oxygen diffusion in a Cr-depleted alloy and consequently enhances degradation by metal dusting. Such microstructure effect can explain the difference in mass losses of 800HT alloy exposed to AP and HP experiments. However, for the HR120 alloy, this does not justify the larger degradation noticed for HP compared to the one observed for AP, as HR120 samples exhibited similar grain sizes.

Despite similar carbon and oxygen activities between the tests, gas mixtures and velocities differ substantially between AP and HP tests. One large difference in gas composition is the water vapor level, much higher at HP. The reduction of metal

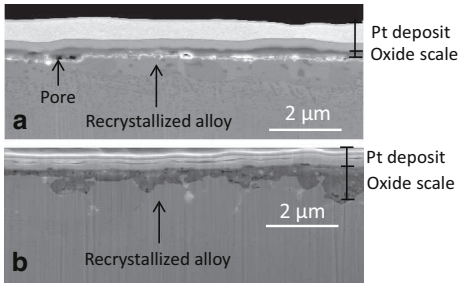

Fig. 6 SEM images, after FIB milling, of the cross-section of the oxide scale of 800HT samples exposed **a** 4000 h at AP and **b** 4966 h at HP

dusting degradation by the addition of H_2O is well known and has already been observed [3, 16–19]. However, the contrary is observed in the present work, i.e. an increase in attack by metal dusting for a H_2O richer environment. Another important difference is the total pressure. Higher total pressures have been found to favor degradation by metal dusting [20–23]. For a given gas mixture, Nishiyama et al. considered that the increase in P_{O_2} resulting in the creation of defects within the oxide scale, associated to the increase in a_c, both due to higher total pressure, favored metal dusting [23]. However, in this study the experiments were designed to reach similar oxygen partial pressures and carbon activities between tests.

SEM observations of 800HT samples corroded in both tests, Fig. 6, revealed different oxide scale morphologies and alloy recrystallization, as the grains below the oxide scale were much finer than in the bulk. While the oxide scale formed at HP seemed to grow inward, the oxide scale developed at AP exhibited pores and a morphology suggesting an outward growth mechanism [24]. Such observations are contrary to the statement made by Nishiyama et al. [23]. Besides, it cannot explain the large gap in pit density between the internal and external sides of a given sample, Fig. 3. Another difference in the test conditions is gas velocity, two orders of magnitude higher for the HP experiment than for the AP test. The large gas velocity, together with a high total pressure, led to large flows of reactive species. In addition, the way the gas was injected in the AP test resulted in a higher gas velocity on the internal side of the samples, where the greatest pit densities were observed. On the contrary, higher pit densities were observed on the external side of samples in the HP test, where the rig design generated a greater gas velocity. The gas velocity is therefore a key parameter to determine the extent of metal dusting attack. The higher it is, the larger the mass loss is. The influence of gas velocity and gas renewal has been discussed in [4] to explain the corrosion ring morphology of pits in 800HT alloy exposed to the AP test. The effect of gas velocity and gas composition on the degradation mechanism of 800HT and HR120 alloys will be discussed thoroughly in a coming paper [24].

Conclusions

Two metal dusting experiments were carried out at 570 °C for more than 6000 h on 800HT and HR120 alloys. The first one was performed at 21 bar with a high gas velocity. The second one was run at atmospheric pressure, under a low gas velocity

and with a gas composition adjusted to reach carbon and oxygen activities similar to those of the high pressure experiment. The dispersion observed for a given alloy regarding mass losses, average incubation times, pit densities and average lateral pit growth rate constants highlights the importance of testing several samples from the same material to get reliable results. For both alloys, incubation times were shorter and mass losses larger at 21 bar. For both metal dusting tests, HR120 alloy underwent greater mass losses and exhibited higher pit densities. The pit density on the sides of the samples varied strongly from one sample to another, for both tests. None of these differences can be explained by the carbon activity alone, since it was similar from one experiment to the other. A fine grain size is usually considered beneficial for metal dusting resistance, as it enhances Cr outward diffusion. In the present study, it reduced the alloy resistance to metal dusting. The large gas velocity of the HP test, associated with a high total pressure, was responsible for shorter incubation times and larger mass losses at 21 bar. A difference in gas velocity also explained the variation in pit density between the sides of the samples.

While many works reported in the literature are based on one sample per alloy, in the present study however, average incubation times and average lateral pit growth rates were determined using three specimens per alloy. This leads to reliable conclusions. However, more samples would be necessary to precise the value intervals, as the measures are scattered.

Acknowledgements This work has been supported by the French National Research Agency through the project ANR SCAPAC 11-RNMP-0016 in partnership with Air Liquide, Veolia VERI, Sedis, University of Lorraine and CIRIMAT Laboratory. Authors thank Xavier Joulia, from LGC laboratory (France), for the calculations made with Simulis Thermodynamics®.

References

1. D. J. Young, J. Zhang, C. Geers and M. Schütze, *Materials and Corrosion* **62**, 2011 (7).
2. H. Yin, J. Zhang and D. J. Young, *Corrosion Science* **51**, 2009 (2983–2993).
3. A. Rouaix-Vande Put, K. A. Unocic, M. P. Brady and B. A. Pint, *Corrosion Science* **92**, 2015 (58).
4. A. Fabas, D. Monceau, C. Josse, P. Lamesle and A. Rouaix-Vande Put, *Corrosion Science* **107**, 2016 (204).
5. A. Fabas, D. Monceau, S. Doublet and A. Rouaix-Vande Put, *Corrosion Science* **98**, 2015 (592).
6. D.-Y. Pend and D. B. Robinson, *Industrial and Engineering Chemistry Fundamentals* **15**, 1976 (59).
7. T. Wada, H. Wada, J. Elliott and J. Chipman, *Metallurgical and Materials Transactions B* **2**, 1971 (2199).
8. J. Zhang and D. Young, *Oxidation of Metals* **70**, 2008 (189).
9. J. Klöwer, H. J. Grabke and E. M. Müller-Lorenz, *Materials and Corrosion* **49**, 1998 (328).
10. H. J. Grabke, E. M. Müller-Lorenz, S. Strauss, E. Pippel and J. Woltersdorf, *Oxidation of Metals* **50**, 1998 (241).
11. J.-W. Park and C. J. Altstetter, *Metallurgical Transactions A* **18**, 1987 (43).
12. J. Swisher and E. T. Turdogan, *Transactions of the Metallurgical Society of AIME* **239**, 1967 (426).
13. S. K. Bose and H. J. Grabke, *Zeitschrift Fur Metallkunde* **69**, 1978 (8).
14. A. R. Paul, K. N. G. Kaimal, M. C. Naik and S. R. Dharwadkar, *Journal of Nuclear Materials* **217**, 1994 (75).
15. S. J. Rothman, L. J. Nowicki and G. E. Murch, *Journal of Physics F-Metal Physics* **10**, 1980 (383).
16. R. F. Hochman, Basic studies of metal deterioration (metal dusting) in carbonaceous atmospheres at elevated temperatures, paper presented at the Proceedings of the 4th International congress on Metal Corrosion, Amsterdam, The Netherlands, September 7–14, (1969, 1972).
17. R. A. Perkins, W. C. Coons and F. J. Radd, *Journal of the Electrochemical Society* **123**, 1976 (733).

18. Z. Zeng, K. Natesan and M. Grimsditch, *Corrosion* **60**, 2004 (632).
19. C. Anghel, E. Hornlund, G. Hultquist and M. Limback, *Applied Surface Science* **233**, 2004 (392).
20. M. Maier, J. F. Norton and P. D. Frampton, *Materials and Corrosion-Werkstoffe Und Korrosion* **49**, 1998 (330).
21. T. P. Levi, N. Briggs, I. E. Minchington and C. W. Thomas, *Materials and Corrosion-Werkstoffe Und Korrosion* **53**, 2002 (239).
22. K. Natesan, Z. Zeng, *Development of Materials Resistant to Metal Dusting Degradation,* Argonne National Laboratory, Technical Report ANL-07/30 (2006).
23. Y. Nishiyama, K. Kitamura and N. Otsuka, *Materials Science Forum* **595–598**, 2008 (649).
24. A. Fabas, D. Monceau, S. Doublet, A. Rouaix-Vande Put, *Corrosion Science*, to be submitted (2017).